Vol. 16, pp. 59–67 (2019)
doi: 10.2142/biophysico.16.0_59

Biophysics and Physicobiology

https://www.jstage.jst.go.jp/browse/biophysico/

Regular Article

Single-particle analysis of full-length human poly(ADP-ribose) polymerase 1

Kenichi Kouyama[1], Kouta Mayanagi[2], Setsu Nakae[1], Yoshisuke Nishi[1], Masanao Miwa[1] and Tsuyoshi Shirai[1]

[1]*Nagahama Institute of BioScience and Technology, Nagahama, Shiga 526-0829, Japan*
[2]*Medical Institute of Bioregulation, Kyushu University, Higashi-ku, Fukuoka 812-8582, Japan*

Received November 22, 2018; accepted December 20, 2018

PolyADP-ribosylation (PARylation) is a posttranslational modification that is involved in the various cellular functions including DNA repair, genomic stability, and transcriptional regulation. PARylation is catalyzed by the poly(ADP-ribose) polymerase (PARP) family proteins, which mainly recognize damaged DNA and initiate repair processes. PARP inhibitors are expected to be novel anticancer drugs for breast and ovarian cancers having mutation in *BRCA* tumor suppressor genes. However the structure of intact (full-length) PARP is not yet known. We have produced and purified the full-length human PARP1 (h-PARP1), which is the major family member of PARPs, and analyzed it with single particle electron microscopy. The electron microscopic images and the reconstructed 3D density map revealed a dimeric configuration of the h-PARP1, in which two ring-shaped subunits are associated with two-fold symmetry. Although the PARP1 is hypothesized to form a dimer on damaged DNA, the quaternary structure of this protein is still controversial. The present result would provide the first structural evidence of the dimeric structure of PARP1.

Corresponding auhor: Tsuyoshi Shirai, Nagahama Institute of BioScience and Technology, 1266 Tamura-cho, Nagahama, Shiga 526-0829, Japan.
e-mail: t_shirai@nagahama-i-bio.ac.jp

Key words: PARP1, DNA repair, electron microscopy, structural biology

PolyADP-ribosylation (PARylation) is a posttranslational modification that is involved in various cellular functions relevant to genomic stability and gene transcription [1]. PARylation is an enzymatic reaction to transfer the ADP-ribose residue of the substrate NAD^+ to various proteins or ADP-ribose residue to form poly(ADP-ribose) polymer (PAR) in both linear and branched chains, by releasing nicotinamide moiety [2,3]. Within the cells, PARylation is mainly catalyzed by poly(ADP-ribose) polymerase (PARP) family enzymes. In humans, for example, 17 PARP family genes have been identified [4].

The synthesis of PAR is known to be a trigger of many cellular activities including base excision repair, DNA replication, DNA transcription, chromatin remodeling, sister chromatid exchanges, centrosome regulation, telomere regulation, cell signal transduction, cell proliferation, carcinogenesis, neurodegeneration, immune protection, ischemia perfusion damage, and cell death [5,6]. Human PARP1 (h-PARP1), the most abundant and interesting member of the PARP family, is known to be involved in base excision repair [7]. h-PARP1 is activated by binding to nicked portion

◀ ***Significance*** ▶

Poly(ADP-ribose) polymerase 1 (PARP1) is the first line sensor of DNA damages in the cell, for which the active quaternary structure is still under debates. Although PARP1 has been thought to form a dimer on damaged DNA for *trans*-PolyADP-ribosylation, several recent studies detected a monomeric DNA recognition and *cis*-PolyADP-ribosylation of PARP1. The present study provides the first structural evidence of dimeric conformation of full-length human PARP1 with single-particle electron microscopy.

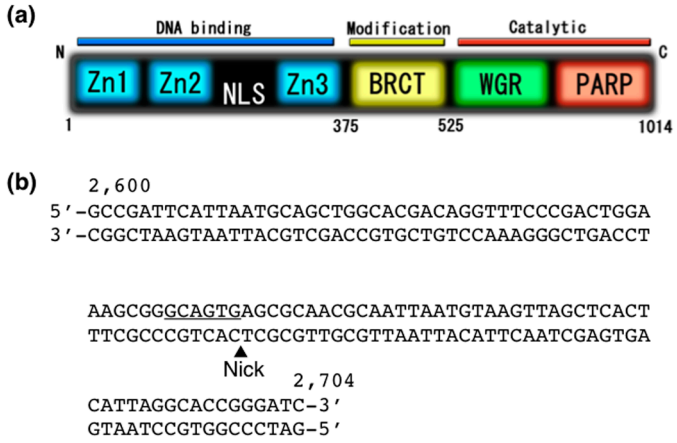

Figure 1 h-PARP1 domains and nicked-DNA ligand. (a) Scheme of h-PARP1 domain organization. NLS is the nuclear localization signal of h-PARP1 at amino acid residues 207–209 and 221–226. (b) Sequence and the nick position (indicated by arrowhead) of the designed dsDNA. The recognition sequence of Nb.BtsI nicking endonuclease is underlined.

(single-stand break) of DNA [8–10], and PARylates acceptor proteins including h-PARP1 itself (automodification) [11]. The DNA repair and chromatin remodeling factors such as XRCC1, DNA polymerase β, and DNA ligase III are then recruited to the PAR, the reaction product of PARylation, and DNA repair process is initiated [12,13].

Recently, the PARP inhibitors attract attentions as anticancer drugs for breast and ovarian cancers, the patients of which often have mutations on BRCA tumor suppressor genes [14]. Inhibition of PARP activity is thought to suppress the DNA repair activity and induce synthetic lethality in the cancer cells. One of such PARP inhibitors, olaparib (Lynparza), has been recently approved as anticancer drug for relapsed ovarian cancers [15].

h-PARP1 is composed of six domains: three zinc finger domains (Zn1, Zn2, and Zn3) for DNA binding or enzyme activation at N-terminal part [16,17], the BRCT automodification domain with BRCA1 C-terminal motif that is important for protein-protein interaction and serves as acceptor sites in automodification. The WGR (tryptophan–glycine–arginine) domain serves as a regulatory domain, and PARP domain with PARylation catalytic activity at C-terminal part [18] (Fig. 1a). To date, the atomic structures of PARP1 have been separately determined for each or two consecutive domains [18–20]. The recent crystal structure analysis revealed the PARP1 model, which composed of three peptide segments corresponding to Zn1, Zn3, and WGR-PARP domains in complex with DNA [21]. This structure was closest to a full-length PARP1 model, but still lacking Zn2 and BRCT domains. Thus, the atomic model of full-length PARP1 is still absent.

Consequently, the structural details of PARP1 activation on damaged DNA are still controversial. One hypothesis claims that the automodification activity requires dimerization of PARP1 molecules, one of which catalyzes PARylation and the other accepts ADP-ribose moiety [19,22–26]. On the other hand, the analyses with small-angle X-ray scattering (SAXS), solution nuclear magnetic resonance (NMR), or atomic force microscopy (AFM) proposed monomeric recognition of the damaged DNA and *cis*(self)-PARylation reaction of PARP1 [21,27–30].

At this point of time, the knowledge of three-dimensional structure of intact PARP1 is not sufficient yet. The structure of intact PARP1 would be essential to determine the structural mode of PARP1 activation on damaged DNAs, and it is also important for developing more effective anticancer drugs. The major hindrance in PARP1 structure analysis is its flexible conformation consisting of multi-domains connected through linkers. Therefore, we designed electron microscopic single particle analysis of full-length h-PARP1. The result demonstrated the first structural evidence of h-PARP1 dimer.

Materials and Methods

Expression and purification of h-PARP1

The cDNA of h-PARP1 mRNA was inserted into pET vector (pET-41a$^{(+)}$, Novagen), in which ubiquitin gene and His tag were added in frame to 5′ and 3′-terminals of h-PARP1 gene, respectively. *Escherichia coli* BL21 cells containing Rosetta 2 plasmid (Novagen) were transformed with the *h-PARP1*-inserted pET vector, and the cells were cultured in 2xYT medium at 37°C until OD_{600} became 0.6. Then, isopropyl-β-D-thiogalactoside (IPTG) was added to the culture and incubation was continued for another 3 h. The cells were collected by centrifugation for 2 min at 4°C and stored at -80°C. Frozen cells were thawed by incubation for 20 min at room temperature by adding BugBuster (Tokyo Chemical Industry Co., Ltd.) and centrifuged for 20 min at 4°C at 16,000×g. The crude extract was purified on HiTrap Heparin HP column (GE Healthcare) with a linear gradient of NaCl between 0 M and 2 M at 0.24 ml/min flow rate [31]. Then,

the protein fractions containing the molecular weight around 118 kDa band (eluted around 625 mM NaCl) were pooled and further purified with 3-aminobenzamide (3-AB) (Tokyo Chemical Industry Co., Ltd.) affinity column. 3-AB-Sepharose column was prepared by binding 3-AB to ECH Sepharose 4B (GE Healthcare) with 1-(3-dimethylaminopropyl)-3-ethylcarbodiimide (Sigma-Aldrich), and was equilibrated with the buffer containing 100 mM Tris-HCl (pH 7.5), 14 mM 2-mercaptoethanol, 0.5 mM ethylenediaminetetraacetic acid, and 0.5 mM phenylmethylsulfonyl fluoride. h-PARP1 was eluted from 3-AB-Sepharose column with a linear gradient of 3-methoxybenzamide (Wako pure chemical corporation) between 0 and 2 mM at 0.24 ml/min flow rate [32]. The fractions were examined by sodium dodecyl sulfate polyacrylamide gel electrophoresis (SDS-PAGE) with a 7.5% (w/v) acrylamide gel, and western blot analysis with anti-h-PARP1 antibody (F2 antibody, Santa Cruz Biotechnology), and those containing the proteins around 118 kDa were further applied to size exclusion chromatography on Superdex 200 (GE Healthcare) using AKTA (GE Healthcare). The protein concentration was determined by using the Lowry method [33].

h-PARP1 enzyme activity assay

The 60 µl mixture, containing purified h-PARP1 (1.6–9.5 µg), 8 mM NAD^+, 8 mM $MgCl_2$, and 2 µg/ml of sonicated salmon sperm DNA in the 3-AB-Sepharose column equilibration buffer was incubated for 30 min at room temperature. The reaction products were analyzed on SDS-PAGE with a 7.5% (w/v) acrylamide gel, and the proteins were detected by western blot analysis with anti-PAR antibody (10H, Merck Millipore) [34,35].

Preparation of dsDNA and nicked-dsDNA

PCR was performed to synthesize 105 bp dsDNA using pET-41a$^{(+)}$ vector as the template. The forward primer (5′-biotin-GCCGATTCATTAATGCAGCTGG-3′), the reverse primer (5′-GATCCCGGTGCCTAATGAGTG-3′), and Pfu Turbo polymerase (Agilent Technologies) were used to amplify from 2600 to 2704 nt positions of pET-41a$^{(+)}$ vector sequence (Fig. 1b). The synthesized 105 bp dsDNA was purified with Wizard SV Gel and PCR Clean-UP System (Promega). A part of the dsDNA was digested for 4 h at 37°C with Nb.BtsI nicking endonuclease (New England Biolabs), which recognized 5′-GCAGTG(nick)-3′ sequence and introduced single-strand break, to produce a 105 bp nicked-dsDNA in the middle of the amplified sequence (Fig. 1b).

Single-particle electron microscopy

The purified h-PARP1 (5 µM) and 105 bp dsDNA (0.18 µM) or nicked-dsDNA (0.18 µM) were mixed and diluted 100 times with the equilibrium buffer for 3-AB-Sepharose column chromatography. A 3 µl aliquot of the sample solution was placed on a hydrophilic carbon membrane grid for 3 min, mixed with 3 drops of 2% (*w*/*v*) uranyl acetate, and dried under room temperature. The images were recorded by a BioScan CCD camera (Gatan) with a pixel size of 5.1 Å/pixel, using a JEM1010 electron microscope (JEOL) operated at an accelerating voltage of 100 kV. The images were corrected with defocus values of –0.5~–1.3 µm. The magnification of the images was calibrated using Tobacco Mosaic Virus as a reference. To minimize the radiation damage of the sample by the electron beam, minimum dose system (MDS) was used.

The images were processed by using EMAN2 [36]. A total of 4971 particles of h-PARP1 (box size 64×64 pixels) were manually selected from the images using the BOXER program, and the CTF (contrast transfer function) was estimated and corrected by phase flipping using e2ctf program. The particle images were class averaged with e2refine2d program, and the initial 3D reconstruction density map was constructed using the common-line method with e2initialmodel tool, and the density map was further refined by assuming C2 symmetry with the e2refine tool. The resolution was evaluated with the Fourier shell correlation (FSC) method by using e2eotest tool.

The molecular model of h-PARP1 was constructed by fitting the crystal/NMR structures of each domain of h-PARP1 into 3D reconstruction density map using UCSF Chimera [37]. The crystal/NMR structures used for modeling were chain A of PDB code 4DQY (Zn1 domain), chain A of 2L31 (Zn2 domain), chain B of 4DQY (Zn3 domain), chain A of 2COK (BRCT domain), chain C (residues 380–492) of 4DQY (WGR domain), and chain C (residues 531–1011) of 4DQY (PARP domain) [21,38]. The visualization of the 3D map and the model were performed with UCSF Chimera [37].

Results and Discussion

Expression and purification of h-PARP1

The full-length *h-PARP1* gene inserted into pET-41a$^{(+)}$ was expressed in BL21 strain of *E. coli*, and purified by combining heparin-Sepharose column chromatography, 3-aminobenzamide (3-AB-Sepharose) affinity column chromatography, and gel filtration. The purification process was monitored by SDS-PAGE and western blot analysis (Fig. 2), and the expression of full-length h-PARP1 protein was confirmed. The ubiquitin-tag was added to N-terminal to the h-PARP1 in the current construct, because expression of h-PARP1 was quite low without the addition of ubiquitin. Since a cleavage of the ubiquitin tag after expression was not successful the ubiquitin tag was not removed in the following analyses.

Although the full-length h-PARP1 (118 kDa) was the major component in the purified preparation (3-AB elution lane in Fig. 2b, indicated with open arrowhead), several low molecular weight components, which reacted with the anti-h-PARP1 antibody (F2 antibody), were also observed. These

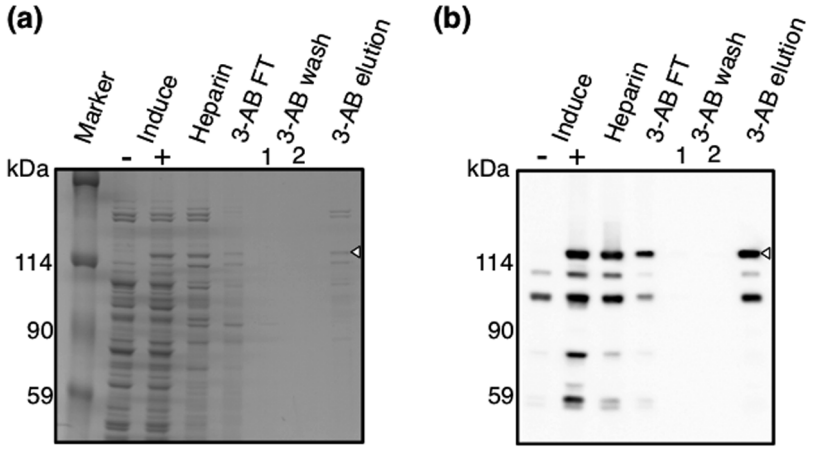

Figure 2 Expression and purification process of full-length h-PARP1. (a) Coomassie brilliant blue (CBB) staining and (b) western blotting images of SDS-PAGE with a 7.5% (*w*/*v*) acrylamide gel of the 0.2% (*v*/*v*) of the representative fraction at each step of the purification process. Marker is the prestained protein marker. Induce – and + indicate without and with induction for 3 h after addition of IPTG, respectively. Heparin is an elution from HiTrap Heparin HP column chromatography. 3-AB FT, wash 1, and wash 2 are the fractions that did not adsorb to 3-AB-Sepharose column, and eluted first and last from the column with washing buffer, respectively. 3-AB elution is the final product eluted from 3-AB-Sepharose column. The predicted full-length h-PARP1 is indicated by open arrowhead in each image.

components seemed to be the products from alternative transcription start sites, because these low molecular weight components were observed in the crude sample without induction (– Induce lane in Fig. 2b). These contaminating products could not be removed through size exclusion chromatography, suggesting they were physically interacting with the full-length h-PARP1, and also could not be suppressed by any attempts in modifying expression conditions thus far.

The enzymatic activity was examined to verify the native structure maintenance of the purified h-PARP1. It is known that active PARP1 catalyzes automodification in the presence of NAD^+ and nicked-dsDNA, and PAR in various chain lengths was covalently bound to the protein, which observed as smear bands with higher molecular weight than intact PARP1 in a gel electrophoresis. In the reaction products, the smear bands above 118 kDa were observed by staining with anti-PAR antibody (Fig. 3). The density of the bands depended on the h-PARP1 amount applied to the reaction, which confirmed the h-PARP1 in the sample was enzymatically active.

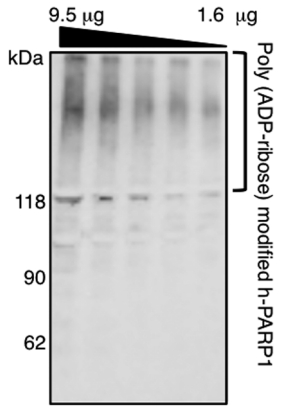

Figure 3 Activity measurement of h-PARP1. Western blot analysis of the automodification reaction products of h-PARP1 using anti-PAR antibody. The protein amounts of 9.5 μg, 6.3 μg, 3.2 μg, 2.1 μg, and 1.6 μg were applied to the reaction from the left to the right lanes. The smear bands above 118 kDa, which are expected to be automodified h-PARP1, are indicated on the right.

The structure of h-PARP1

The h-PARP1 was mixed with dsDNA or nicked-dsDNA and analyzed by transmission electron microscopy after negative staining with uranyl acetate. Judged form the electron micrograms, monodispersity of the particles was low, which might reflect the contamination of the low molecular weight components (Fig. 4). The typical particle shape was connected two-rings (Fig. 4a inset). Because of the low monodispersity, the particles were picked up completely manually through visual inspections with e2boxer tool in EMAN2 [36].

The observed particles in the presence of dsDNA (Fig. 4a) or nicked-dsDNA (Fig. 4b) did not differ significantly, and no significant density of DNA was observed in either image. The class averages of both particles, obtained separately, did not show significant difference to each other. Thus, both the dsDNA and nicked-dsDNA appeared to be unbound to the proteins. Therefore, in order to increase the number of particles, the following analyses were performed by combining the particle images in the presence of dsDNA and nicked-dsDNA.

A total of 4,791 particles were manually selected and classified into 31 class averages. Most of the class average

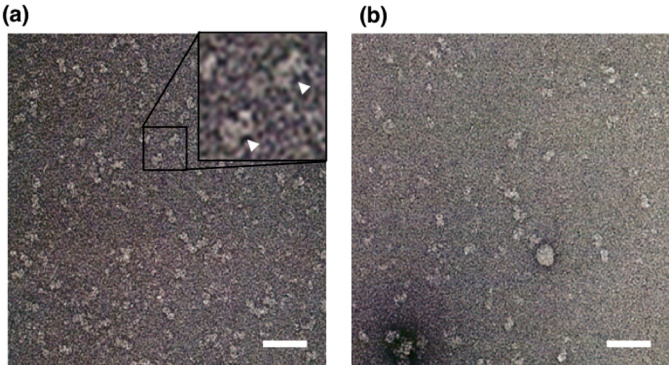

Figure 4 Electron micrograph of h-PARP1. Examples of micrograms of h-PARP1 sample with (a) nicked-dsDNA and (b) dsDNA. The inset in plate (a) shows an enlarged view of the predicted h-PARP1 dimer particles (indicated by arrowhead). Scale bars represent 50 nm.

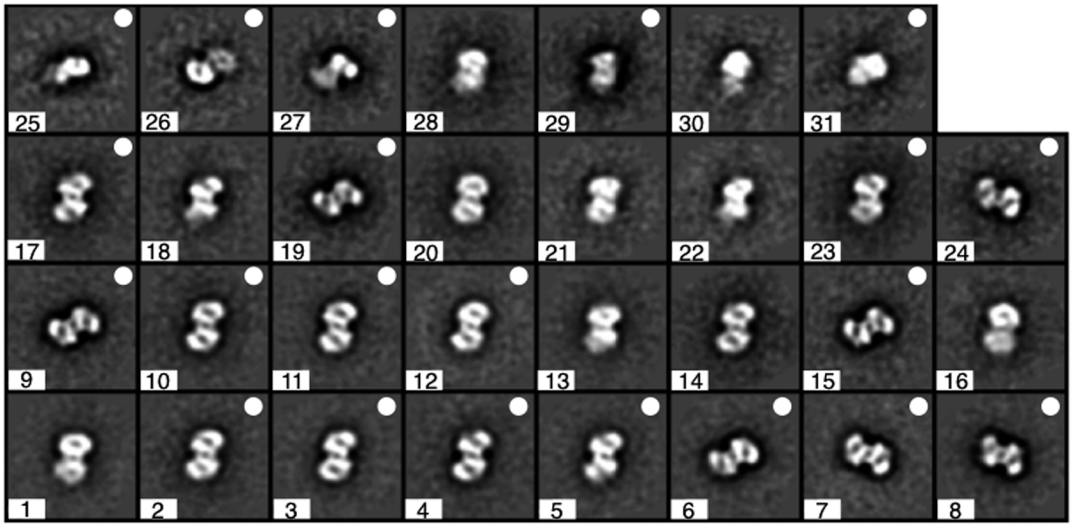

Figure 5 Class average images of h-PARP1. Class averages of h-PARP1 particle. The classes indicated with white dot were used for the initial model construction.

showed two-fold symmetry, by which ring-shaped subunits were related (Fig. 5). From these class averages, 21 were selected to construct the initial model without hypothesizing symmetry (C1), and further refined by referring to all particle images. Since the reconstructed density map clearly indicated two-fold symmetry, the density map was submitted to the second cycle refinement by assuming C2 symmetry (Fig. 6). The Fourier shell correlation (FSC) curve from the (standard) even/odd test was calculated, and the resolution of the density map was evaluated to be 28 Å for the FSC=0.5 criteria (Fig. 7a). The Euler angle (the viewing angle) distributions of particles used for the final map showed a bias to the viewing angles along the symmetry axis, as was anticipated from the class averages (Fig. 7b). Though a uniform distribution of the angles is preferred for a perfect 3D reconstruction, the viewing angles normal to the symmetry axis, required for a correct 3D structure analysis, were obtained to a certain extent for this sample. The

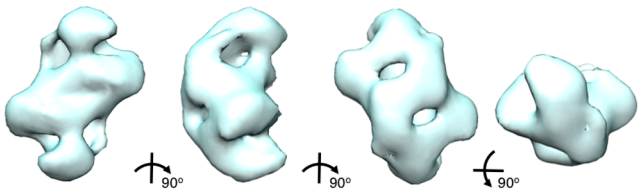

Figure 6 3D reconstruction of h-PARP1 density map. Density map of h-PARP1 dimer in (a) front, (b) side, (c) back, and (d) top views.

final density map demonstrated a structure, in which two subunits were contacting through relatively larger domains close to the center, and smaller domains were connected to the central domain and placed distal to the two-fold axis (Fig. 6). Thus the result suggested the dimeric structure of full-length h-PARP1.

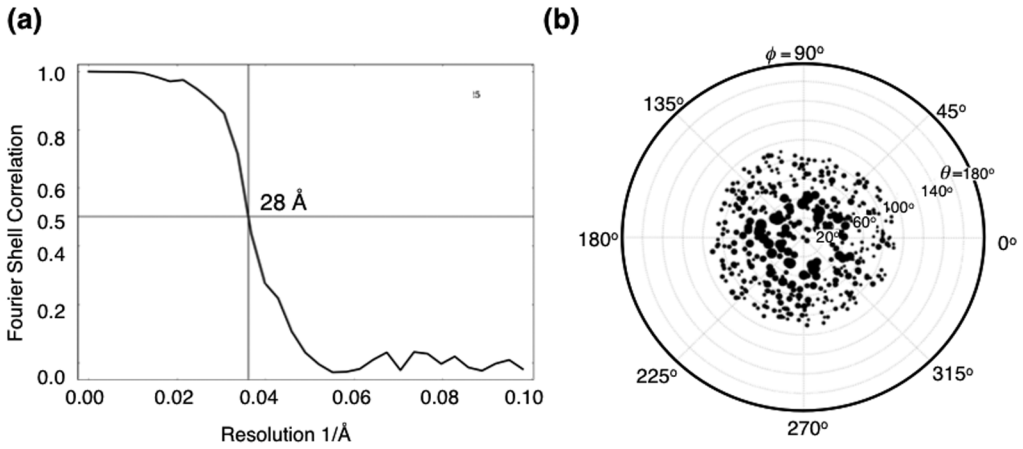

Figure 7 FSC and Euler angle distributions. (a) Fourier shell correlation (vertical axis) from the standard even/odd test is plotted against wave number (horizontal axis). (b) Euler angle distributions of the particle viewing angles.

Fitting molecular models into h-PARP1 density map

The fitting of the separately determined domain structures of h-PARP1 into the obtained density map was attempted [18–21], since the full-length model of h-PARP1 is still absent. Among these structures, the crystal structure (PDB 4DQY) of the complex of Zn1 (chain A), Zn3 (chain B), and WGR-PARP (chain C) domains, *i.e.*, lacking Zn2 and BRCT domains, was most close to the full-length h-PARP1 [21]. In spite of several attempts, however, the crystal structure could not fit well as a whole to the density map, suggesting that a rearrangement of the domains occurred.

Therefore, each domain, including Zn2 (PDB 2L31) and BRCT (PDB 2COK) domains, was fitted into the map one by one by considering the connectivity of domains along the primary structure. As a starting model, two PARP domains were symmetrically placed in the central part of the map near the two-fold axis, because the single PARP1 domain, consisting of 353 amino acid residues (residues 662–1014), was the largest among the domains, and the map except for the central part appeared to be small to accommodate this domain. The WGR and BRCT domains were deployed on the density near the PARP domain, and these domains also took part in the inter-subunit interface. The DNA binding domains, namely Zn1, Zn2, and Zn3, were arranged in the densities distal to the two-fold axis (Fig. 8a). No apparent density for the N-terminal ubiquitin tag and dsDNA or nicked-dsDNA was observed.

The distances between terminal residues of the domains in the final model were as follows (in parentheses are the number of unmodeled linker resides between domains): Zn1–Zn2 16 Å (13), Zn2–Zn3 15 Å (11), Zn3–BRCT 37 Å (22), BRCT–WGR 20 Å (40), and WGR–PARP 36 Å (19, the corresponding distance in the crystal structure PDB 4DQY was also 36 Å). The correlation coefficient between the experimental and the model-derived density maps was 0.87. The presented density map was contoured so that the volume became ~302,000 Å^3, which was evaluated from the molecular weight of h-PARP1 dimer including the N-terminal ubiquitin tags (118×2 kDa) by assuming canonical density of proteins (1.3 g/cm^3).

Although the current fitting of the models should remain tentative due to the low resolution and lack of experimental allocation of domains by labeling experiments, the observed density map demonstrated that the volume was large enough for accommodating the domains of two full-length h-PARP1 molecules. The density map supported a dimeric structure of h-PAPR1, which provides the first structural evidence of the quarterly structure of full-length h-PARP1.

Implications from dimeric h-PARP1 model

The stoichiometry of PARP1 in recognizing various damaged DNAs, such as nicked, double-strand break, or abasic sites, is still under debates [21,29,30]. The dimeric PARP1 structure and *trans*(inter molecular)-PARylation between associated PARP1 molecules have been proposed mainly based on the enzymatic reaction kinetics. The automodification rate increased with second order kinetics as the calf thymus or chicken PARP1 concentration increased [23,26]. Also the enzymatically inactive h-PARP1 mutant was PARylated when the wild-type co-existed [25]. In the analyses of PARP1 domain(s), it was reported that the Zn1–Zn2 DNA binding domains of h-PARP1 bound to DNA as a dimer [19,24], and WGR-PARP domains of chicken PARP1 formed a hetero dimer with the full-length PARP1 [26].

The recent studies, however, supported monomeric recognition of damaged DNA by PARP1. The small-angle X-ray scattering experiment demonstrated the N-terminal domains of h-PARP1, which contained DNA binding and BRCT domains, bound to DNA as a monomer [27]. The complex of Zn1, Zn2, and WGR-PARP domains recognized the double-strand breaks of DNA as a monomer in the crystal structure [21,28]. The analyses of PARP1 activation on single-strand

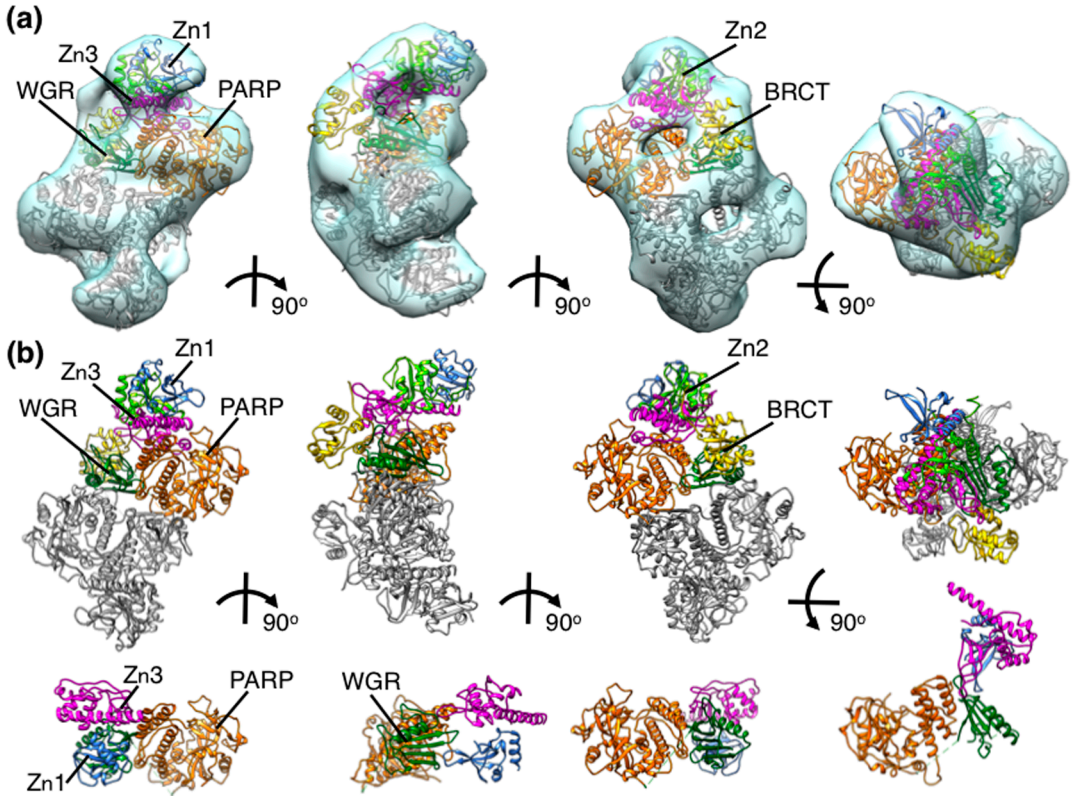

Figure 8 Model fitting to h-PARP1 density map. (a) Fitting of the crystal/NMR structures of Zn1 (blue), Zn2 (yellow green), Zn3, (magenta), BRCT (yellow), WGR (green), and PARP (orange) domains into the density map of h-PARP1 dimer. (b) The same models without density map are shown on the top. The crystal structure (PDB 4DQY), which is superimposed on the upper subunit in the dimer model at PARP domain, is shown on the bottom for a comparison of domain organizations. The domain colors of the crystal structure are same as the dimer model.

DNA breaks by combining solution NMR and molecular modeling proposed a model, in which single PARP1 molecule recognize the DNA damage through Zn1-Zn2 DNA-binding domains, and stepwise self-assembly of other domains enables *cis*(intra molecular)-PARylation reaction [29]. Also the volume estimation with AFM detected that the MBP-tagged full-length h-PARP1 binds to abasic sites of DNA as a monomer [30].

Putting together, these reports would be summarized into two points. First, no structure analysis has been ever reported, either by X-ray crystallography or electron microscopy, for full-length PARP1, particularly a molecule that has all of the C-terminal domains (BRCT, WGR, and PARP). In the full-length h-PARP1 dimer model of this study, the PARP domain provides the major interface between two subunits of h-PARP1, but WGR and BRCT domains are also involved in the interface. The DNA binding domains are situated at the opposite distal part of the dimer, and are not involved in the interaction between the subunits. This model suggests that PARP, WGR, and BRCT domains are necessary for dimer formation, and it might explain why thus far reported structures of PARP1 had monomeric structure.

Second, physical interaction between PARP1 molecules tends to be observed in absence of DNA. The gel-filtration, native-PAGE, and cross-linking experiments have revealed that the bovine-PARP1 formed dimer under high concentration in the absence of DNA [22]. It was also demonstrated that the WGR-PARP domains of chicken PARP1 formed a hetero dimer with the full-length PARP1 without DNA [26]. In the present study, no significant density for dsDNA or nicked-dsDNA was observed. It would suggest that the dimeric structure of h-PARP1 is a DNA-unbound form, probably in the resting state, and the subunit would dissociate to recognize damaged DNAs. The initial process of damaged DNA recognition of PARP1 is thought to be the binding of Zn1-Zn2 domains to a single-strand break point, and this process involves substantial change in the spatial arrangement of the domains [29,30]. In the dimer model of h-PARP1, these domains are allocated to the peripherals of the complex and easily accessible to DNA, although the domain spatial arrangements are different from that of the crystal structure (Fig. 8b).

In summary, the present study provides the first structural evidence of dimeric h-PARP1. The tentative model suggested the dimer would represent a DNA-unbound configuration, and explain why it has not been observed before, because no structure analysis has been reported for a full-length PARP1 without DNA molecule thus far. The physio-

logical significance of the dimer structure, along with improvement of the structural model in higher-resolution density map, would be necessary to further elucidate the damaged DNA recognition process of h-PARP1.

Acknowledgement

This work was partly performed in the Cooperative Research Project Program of the Medical Institute of Bioregulation, Kyushu University. We thank Dr. Mitsuko Masutani of National Cancer Center Research Institute for giving us the expression vector of h-PARP1, and Dr. Kazuo Kamemura of Nagahama Institute of Bio-Science and Technology for suggestion of constructing recombinant h-PARP1. This work was partly supported by Grant-in-Aid from Ministry of Education, Culture, Sports, Science and Technology, Japan.

Conflicts of Interest

The authors declare that they have no conflict of interest.

Author contribution

Y. N. constructed h-PARP1 expression vector. K. K., S. N., and M. M. prepared h-PARP1 and DNA samples. K. K., K. M., and T. S. conducted single-particle electron microscopy experiments. K. K., M. M., and T. S. wrote the manuscript. T. S. supervised the study.

References

[1] Gibson, B. A. & Kraus, W. L. New insights into the molecular and cellular functions of poly(ADP-ribose) and PARPs. *Nat. Rev. Mol. Cell Biol.* **13**, 411–424 (2012).
[2] Sugimura, T. Poly(adenosine diphosphate ribose). *Prog. Nucleic Acid Res. Mol. Biol.* **13**, 127–151 (1973).
[3] Miwa, M., Ishihara, M., Takishima, S., Takasuka, N., Maeda, M., Yamaizumi, Z., *et al.* The branching and linear portions of poly(adenosine diphosphate ribose) have the same alpha (1 leads to 2) ribose-ribose linkage. *J. Biol. Chem.* **256**, 2916–2921 (1981).
[4] Amé, J. C., Spenlehauer, C. & de Murcia, G. The PARP superfamily. *Bioessays* **26**, 882–893 (2004).
[5] Schreiber, V., Dantzer, F., Amé, J. C. & de Murcia, G. Poly(ADP-ribose): novel functions for an old molecule. *Nat. Rev. Mol. Cell Biol.* **7**, 517–528 (2006).
[6] Miwa, M. & Masutani, M. PolyADP-ribosylation and cancer. *Cancer Sci.* **98**, 1528–1535 (2007).
[7] Durkacz, B. W., Omidiji, O., Gray, D. A. & Shall, S. (ADP-ribose)n participates in DNA excision repair. *Nature* **283**, 593–596 (1980).
[8] Benjamin, R. C. & Gill, D. M. Poly(ADP-ribose) synthesis in vitro programmed by damaged DNA. A comparison of DNA molecules containing different types of strand breaks. *J. Biol. Chem.* **255**, 10502–10508 (1980).
[9] Menissier-de Murcia, J., Molinete, M., Gradwohl, G., Simonin, F. & de Murcia, G. Zinc-binding domain of poly(ADP-ribose) polymerase participates in the recognition of single strand breaks on DNA. *J. Mol. Biol.* **210**, 229–233 (1989).
[10] Le Cam, E., Fack, F., Menissier-de Murcia, J., Cognet, J. A., Barbin, A., Sarantoglou, V., *et al.* Conformational analysis of a 139 base-pair DNA fragment containing a single-stranded break and its interaction with human poly(ADP-ribose) polymerase. *J. Mol. Biol.* **235**, 1062–1071 (1994).
[11] Althaus, F. R. & Richter, C. ADP-ribosylation of proteins. Enzymology and biological significance. *Mol. Biol. Biochem. Biophys.* **37**, 1–237 (1987).
[12] Masson, M., Niedergang, C., Schreiber, V., Muller, S., Menissier-de Murcia, J. & de Murcia, G. XRCC1 is specifically associated with poly(ADP-ribose) polymerase and negatively regulates its activity following DNA damage. *Mol. Cell. Biol.* **18**, 3563–3571 (1998).
[13] Simbulan-Rosenthal, C. M., Rosenthal, D. S. & Smulson, M. E. Purification and characterization of poly(ADP-ribosyl)ated DNA replication/repair complexes. *Methods Mol. Biol.* **780**, 165–190 (2011).
[14] Kraus, W. L. PARPs and ADP-Ribosylation: 50 Years ... and Counting. *Mol. Cell* **58**, 902–910 (2015).
[15] Sonnenblick, A., de Azambuja, E., Azim, H. A., Jr. & Piccart, M. An update on PARP inhibitors—moving to the adjuvant setting. *Nat. Rev. Clin. Oncol.* **12**, 27–41 (2015).
[16] Langelier, M. F., Planck, J. L., Roy, S. & Pascal, J. M. Crystal structures of poly(ADP-ribose) polymerase-1 (PARP-1) zinc fingers bound to DNA: structural and functional insights into DNA-dependent PARP-1 activity. *J. Biol. Chem.* **286**, 10690–10701 (2011).
[17] Langelier, M. F., Ruhl, D. D., Planck, J. L., Kraus, W. L. & Pascal, J. M. The Zn3 domain of human poly(ADP-ribose) polymerase-1 (PARP-1) functions in both DNA-dependent poly(ADP-ribose) synthesis activity and chromatin compaction. *J. Biol. Chem.* **285**, 18877–18887 (2010).
[18] Iwashita, A., Hattori, K., Yamamoto, H., Ishida, J., Kido, Y., Kamijo, K., *et al.* Discovery of quinazolinone and quinoxaline derivatives as potent and selective poly(ADP-ribose) polymerase-1/2 inhibitors. *FEBS Lett.* **579**, 1389–1393 (2005).
[19] Ali, A. A. E., Timinszky, G., Arribas-Bosacoma, R., Kozlowski, M., Hassa, P. O., Hassler, M., *et al.* The zinc-finger domains of PARP1 cooperate to recognize DNA strand breaks. *Nat. Struct. Mol. Biol.* **19**, 685–692 (2012).
[20] Langelier, M. F., Servent, K. M., Rogers, E. E. & Pascal, J. M. A third zinc-binding domain of human poly(ADP-ribose) polymerase-1 coordinates DNA-dependent enzyme activation. *J. Biol. Chem.* **283**, 4105–4114 (2008).
[21] Langelier, M. F., Planck, J. L., Roy, S. & Pascal, J. M. Structural basis for DNA damage-dependent poly(ADP-ribosyl)ation by human PARP-1. *Science* **336**, 728–732 (2012).
[22] Bauer, P. I., Buki, K. G., Hakam, A. & Kun, E. Macromolecular association of ADP-ribosyltransferase and its correlation with enzymic activity. *Biochem. J.* **270**, 17–26 (1990).
[23] Mendoza-Alvarez, H. & Alvarez-Gonzalez, R. Poly(ADP-ribose) polymerase is a catalytic dimer and the automodification reaction is intermolecular. *J. Biol. Chem.* **268**, 22575–22580 (1993).
[24] Pion, E., Bombarda, E., Stiegler, P., Ullmann, G. M., Mely, Y., de Murcia, G., *et al.* Poly(ADP-ribose) polymerase-1 dimerizes at a 5′ recessed DNA end in vitro: a fluorescence study. *Biochemistry* **42**, 12409–12417 (2003).
[25] Altmeyer, M., Messner, S., Hassa, P. O., Fey, M. & Hottiger, M. O. Molecular mechanism of poly(ADP-ribosyl)ation by PARP1 and identification of lysine residues as ADP-ribose acceptor sites. *Nucleic Acids Res.* **37**, 3723–3738 (2009).
[26] Mendoza-Alvarez, H. & Alvarez-Gonzalez, R. The 40 kDa carboxy-terminal domain of poly(ADP-ribose) polymerase-1

forms catalytically competent homo- and heterodimers in the absence of DNA. *J. Mol. Biol.* **336**, 105–114 (2004).
[27] Lilyestrom, W., van der Woerd, M. J., Clark, N. & Luger, K. Structural and biophysical studies of human PARP-1 in complex with damaged DNA. *J. Mol. Biol.* **395**, 983–994 (2010).
[28] Langelier, M. F. & Pascal, J. M. PARP-1 mechanism for coupling DNA damage detection to poly(ADP-ribose) synthesis. *Curr. Opin. Struct. Biol.* **23**, 134–143 (2013).
[29] Eustermann, S., Wu, W. F., Langelier, M. F., Yang, J. C., Easton, L. E., Riccio, A. A., *et al.* Structural Basis of Detection and Signaling of DNA Single-Strand Breaks by Human PARP-1. *Mol. Cell* **60**, 742–754 (2015).
[30] Liu, L., Kong, M., Gassman, N. R., Freudenthal, B. D., Prasad, R., Zhen, S., *et al.* PARP1 changes from three-dimensional DNA damage searching to one-dimensional diffusion after auto-PARylation or in the presence of APE1. *Nucleic Acids Res.* **45**, 12834–12847 (2017).
[31] Amé, J. C., Kalisch, T., Dantzer, F. & Schreiber, V. Purification of recombinant poly(ADP-ribose) polymerases. *Methods Mol. Biol.* **780**, 135–152 (2011).
[32] Burtscher, H. J., Auer, B., Klocker, H., Schweiger, M. & Hirsch-Kauffmann, M. Isolation of ADP-ribosyltransferase by affinity chromatography. *Anal. Biochem.* **152**, 285–290 (1986).
[33] Lowry, O. H., Rosebrough, N. J., Farr, A. L. & Randall, R. J. Protein measurement with the Folin phenol reagent. *J. Biol. Chem.* **193**, 265–275 (1951).
[34] Yoshihara, K., Hashida, T., Yoshihara, H., Tanaka, Y. & Ohgushi, H. Enzyme-bound early product of purified poly(ADP-ribose) polymerase. *Biochem. Biophys. Res. Commun.* **78**, 1281–1288 (1977).
[35] Kawamitsu, H., Hoshino, H., Okada, H., Miwa, M., Momoi, H. & Sugimura, T. Monoclonal antibodies to poly(adenosine diphosphate ribose) recognize different structures. *Biochemistry* **23**, 3771–3777 (1984).
[36] Ludtke, S. J., Baldwin, P. R. & Chiu, W. EMAN: semiautomated software for high-resolution single-particle reconstructions. *J. Struct. Biol.* **128**, 82–97 (1999).
[37] Pettersen, E. F., Goddard, T. D., Huang, C. C., Couch, G. S., Greenblatt, D. M., Meng, E. C., *et al.* UCSF Chimera—a visualization system for exploratory research and analysis. *J. Comput. Chem.* **25**, 1605–1612 (2004).
[38] Eustermann, S., Videler, H., Yang, J. C., Cole, P. T., Gruszka, D., Veprintsev, D., *et al.* The DNA-binding domain of human PARP-1 interacts with DNA single-strand breaks as a monomer through its second zinc finger. *J. Mol. Biol.* **407**, 149–170 (2011).